

# Energetics of drop and bubble deformation with application to turbulent breakup

Alberto Vela-Martín<sup>1†</sup>, Marc Avila<sup>2</sup>

<sup>1</sup>School of Aeronautics, Universidad Politécnica de Madrid, 28040 Madrid, Spain

<sup>2</sup>Center of Applied Space Technology and Microgravity (ZARM) University of Bremen, 28359 Bremen

(Received xx; revised xx; accepted xx)

Drop breakup in fluid flows is investigated here as an exchange between the fluid's kinetic energy and the drop's surface energy. We show analytically that this energetic exchange is governed only by the action of the rate-of-strain tensor on the surface of the drop, more specifically, by a term analogous to vortex stretching. Our formulation allows to isolate the energetic exchange due to the relaxation of the drop, from the action of velocity fluctuations leading to breakup. We perform direct numerical simulations of single drops in isotropic homogeneous turbulence and show that an important contribution to breakup arises from the stretching of the fluid-fluid interface by velocity fluctuations away from the drop surface. This mechanism is approximately independent of the Weber number, whereas the dynamics inside (and close to) the drop only contribute to breakup for sufficiently large Weber numbers.

**Key words:** turbulence, drop breakup, diffuse-interface methods

## 1. Introduction

The breakup of drops and bubbles in turbulent flows is a key process in many natural phenomena and industrial applications. Understanding the physical mechanisms that lead to breakup is essential to develop accurate predictive models (Hakansson 2019). Many commonly used breakup models rely on an energetic description of the phenomena introduced by Kolmogorov (1949) and Hinze (1955), in which the ‘impact’ of turbulent eddies on the surface of the drop increases the surface energy until a given threshold is reached and the drop breaks. In these models the kinetic energy of turbulent eddies and their arrival frequency are typically used as characteristic model parameters (see e.g. Lasheras *et al.* 2002; Liao & Lucas 2009, for reviews). This approach to modeling breakup is convenient because it lumps the complexity of drop-turbulence interactions into model parameters, but it depends on the validity of the model assumptions about the energetic exchange between the drop and the turbulent flow. To date, the physical mechanisms underlying this energetic exchange remain poorly understood and laboratory experiments to validate and to parametrize these (and other) models are extremely challenging (see e.g. Risso & Fabre 1998; Eastwood *et al.* 2004; Maaß & Kraume 2012). This hinders accurate predictions of drop breakup and drop-size distributions even in simple turbulent flows (Aiyer *et al.* 2019).

A convenient framework to analyze the energetic exchange between the kinetic energy

† Email address for correspondence: albertovela@gmail.com

of the fluids and the surface energy of a drop (or more precisely the free energy of the fluid mixture) is given by the Cahn–Hilliard–Navier–Stokes equations (Jacqmin 1999). In these equations the interface is of finite thickness  $\epsilon$ , but as  $\epsilon \rightarrow 0$  the sharp-interface limit is recovered (with the classical stress balance at the infinitesimal fluid–fluid interface, see Magaletti *et al.* 2013). In this paper, we exploit this framework to show that this energetic exchange is solely described by the action of the rate-of-strain tensor on the surface of the drop. Moreover, we decompose the rate-of-strain tensor to distinguish between inner and outer contributions and apply this decomposition to shed light on the mechanisms of drop breakup in homogeneous isotropic turbulence.

## 2. Energy exchange between kinetic energy and surface energy

We consider the incompressible Navier–Stokes (NS) equations coupled to the Cahn–Hilliard (CH) equations,

$$\rho(\partial_t u_i + u_j \partial_j u_i) = -\partial_i p + 2\partial_j \mu S_{ij} + f_i - c \partial_i \phi, \quad \partial_t c + u_j \partial_j c = \kappa \partial_{kk} \phi, \quad (2.1)$$

which, together with the incompressibility constraint,  $\partial_i u_i = 0$ , describe the evolution of an immiscible binary mixture of incompressible fluids (Jacqmin 1999). Here  $u_i$  is the  $i$ -th component of the velocity vector,  $p$  is a modified pressure,  $S_{ij} = \frac{1}{2}(\partial_i u_j + \partial_j u_i)$  is the rate-of-strain tensor and  $f_i$  is a body-force term per unit volume. Repeated indices imply summation, and we consider periodic boundary conditions. The concentration of each component in the mixture is represented by  $c$ , where  $c = \pm 1$  are the pure components. The density  $\rho$  and dynamic viscosity  $\mu$  of the fluid mixture depend on  $c$  and the immiscibility is modelled through a chemical potential,

$$\phi = \beta(c^2 - 1)c - \alpha \partial_{kk} c. \quad (2.2)$$

The numerical parameters  $\alpha$  and  $\beta$  determine the typical width of the fluid–fluid interface,  $\epsilon = 4\sqrt{2\alpha/\beta}$ , and the mobility,  $\kappa$ , determines its typical relaxation time. When these parameters are fixed appropriately (Magaletti *et al.* 2013), the interface is consistently close to the equilibrium profile,  $c_{eq}(x) = \tanh(4x/\epsilon)$ , and the surface tension reads

$$\sigma = \alpha \int_{-\infty}^{+\infty} (\partial_i c_{eq})^2 dx = \frac{4}{3\sqrt{2}} \sqrt{\alpha\beta}, \quad (2.3)$$

where  $x$  is the spatial coordinate in the direction normal to the interface.

### 2.1. Governing equations of the kinetic energy and the surface energy

The evolution equation of the kinetic energy of the flow is obtained by taking the dot product of the NS equations with  $u_i$ . Invoking incompressibility,  $-c \partial_i \phi$  is converted into  $\phi \partial_i c$  plus an extra term that is absorbed into the modified pressure,  $p' = p + c\phi$ , and the equation reads

$$\partial_t e + u_j \partial_j e = \partial_i (u_i p' + 2\mu u_j S_{ij}) - 2\mu S_{ij} S_{ij} + u_i \phi \partial_i c + u_i f_i, \quad (2.4)$$

where  $e = 1/2 \rho u_i u_i$  is the turbulent kinetic energy per unit volume. The only terms contributing on average to the total kinetic energy budget are the local kinetic energy dissipation,  $2\mu S_{ij} S_{ij}$ , the power input,  $u_i f_i$ , and the energetic exchange between the kinetic energy and the surface energy,  $\phi u_i \partial_i c$ . This term acts in the fluid–fluid interface and is also present, with changed sign, in the evolution equation for the free energy, which is obtained by multiplying the CH equation by the chemical potential,

$$\partial_t h + u_j \phi \partial_j c = \kappa \phi \partial_{kk} \phi, \quad (2.5)$$

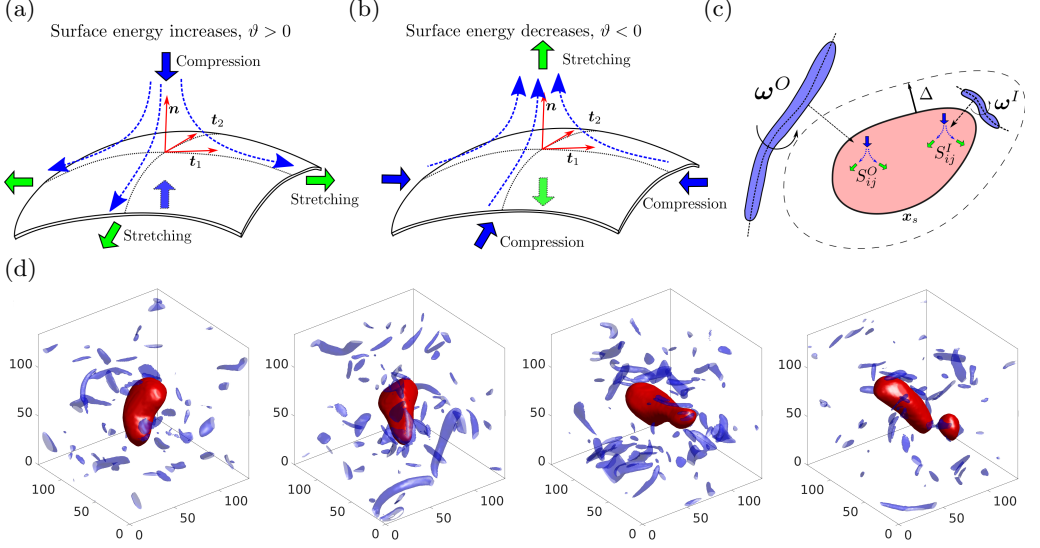


FIGURE 1. (a,b) Schematic representation of the mechanism that generates (a) positive and (b) negative increments of the surface energy due to the compression or stretching of the drop surface, where  $\mathbf{n}$  is the orthogonal vector normal to the interface,  $\mathbf{t}^1$  and  $\mathbf{t}^2$  are vectors parallel to the surface, and  $\vartheta = -\sigma n_i S_{ij} n_j$ . Blue and green arrows indicate the compressive and stretching directions of the rate-of-strain tensor at the surface, and dotted lines are the streamlines of the velocity field with respect to the surface. (c) Decomposition of the rate-of-strain acting on the drop surface on the outer and inner contributions. (d) Temporal evolution of a drop at  $We = 1.8$ . The frame is fixed at the center of the drop, and the time of the snapshots corresponds, from left to right, to  $t/t_d = 2.0, 2.9, 3.9, 4.8$ , and  $5.1$ . Blue isosurfaces denote vorticity with magnitude  $|\boldsymbol{\omega}| = 2.6\langle|\boldsymbol{\omega}|\rangle$ . The size of the computational box is marked in Kolmogorov units.

where  $h = \beta/4(c^2 - 1)^2 + \alpha/2(\partial_k c)^2$  is the free energy per unit volume. We seek to reveal the fundamental mechanism that drives the energetic exchange between the kinetic energy and the surface energy by transforming (2.5) into an advection equation for  $h$ . By decomposing the product  $\phi \partial_i c$  and operating on the partial derivatives, we find the relation

$$\phi \partial_i c = \partial_i h - \alpha \partial_k \tau_{ik}, \quad (2.6)$$

where  $\tau_{ik} = \partial_i c \partial_k c$  is a Korteweg stress tensor. Substituting this expression in the kinetic energy equation and the free energy equation, we obtain

$$\begin{aligned} \partial_t e + u_j \partial_j e &= \partial_i \Psi_i - 2\mu S_{ij} S_{ij} - \alpha u_i \partial_j \tau_{ij} + u_i f_i, \\ \partial_t h + u_j \partial_j h &= \kappa \phi \partial_{kk} \phi + \alpha u_i \partial_j \tau_{ij}, \end{aligned} \quad (2.7)$$

where  $\Psi_i = u_i(p' + h) + 2\mu u_j S_{ij}$ . The energetic exchange is described by the action of a stress tensor,  $\tau_{ij}$ , and the free energy equation has been transformed into an advection equation, where the first term in the right-hand side represents the diffusive action of the chemical potential, and the second term the interaction of the interface with the velocity field.

## 2.2. The physical mechanism leading to variations of the surface energy

The energy-exchange term can be further expanded into

$$\alpha u_i \partial_j \tau_{ij} = \alpha \partial_j (u_i \tau_{ij}) - \alpha S_{ij} \tau_{ij}. \quad (2.8)$$

The first term in the right-hand side represents the divergence of a flux and vanishes in the mean. Due to the symmetric form of  $\tau_{ij}$ , only the symmetric part of the velocity gradient tensor, the rate-of-strain tensor  $S_{ij} = 1/2(\partial_i u_j + \partial_j u_i)$ , interacts with  $\tau_{ij}$ . Considering that the components of the vector normal to the interface are  $n_i = \partial_i c / \gamma$ , where  $\gamma = \sqrt{(\partial_k c)^2}$ , we rewrite the exchange term as  $-\alpha \gamma^2 n_i S_{ij} n_j$ . This term describes the change in free energy per unit volume; by integrating normal to the interface we transform it into an energy change per unit surface,

$$\vartheta = -\sigma n_i S_{ij} n_j. \quad (2.9)$$

Here we have assumed that the interface is in equilibrium (so that eq. (2.3) holds) and that neither  $\mathbf{n}$  nor  $S_{ij}$  change substantially across the interface width. Both assumptions are fulfilled in the sharp-interface limit (Magaletti *et al.* 2013).

In this form, the exchange term is described by the stretching or contraction of the interface thickness by the rate-of-strain tensor. This result may be difficult to interpret from a physical and geometrical perspective, because the width of the interface between immiscible fluids is of molecular scale. From incompressibility it follows that  $S_{ij} \delta_{ij} = 0$ , where  $\delta_{ij}$  is the Kronecker delta, and  $S_{ij} n_j n_i = S_{ij} (n_j n_i - \delta_{ij})$ . Now we can reformulate (2.9) in terms of any pair of orthonormal vectors parallel to the surface,  $\mathbf{t}^1$  and  $\mathbf{t}^2$ ,

$$\vartheta = \sigma (t_k^1 S_{kj} t_j^1 + t_k^2 S_{kj} t_j^2), \quad (2.10)$$

where we have considered that,  $n_j n_i - \delta_{ij} = -t_i^1 t_j^1 - t_i^2 t_j^2$ . This expression shows that the surface energy increases as a consequence of the stretching of the surface area by the rate-of-strain tensor, where  $d_t \log \delta A = (t_k^1 S_{kj} t_j^1 + t_k^2 S_{kj} t_j^2)$  is the growth rate of an infinitesimal area,  $\delta A$ , on the surface of the drop. The opposite situation is also possible, and the decrements of the surface energy are related to the contraction of the surface area. In figure 1(a,b) we show a schematic representation of these mechanisms.

By taking volume and surface averages of (2.7), we obtain an equation for the evolution of the total kinetic energy and the total surface energy,  $\mathcal{E} = \langle e \rangle_V$  and  $\mathcal{H} = \langle h \rangle_V$ ,

$$d_t \mathcal{H} = \kappa \langle \phi \partial_{kk} \phi \rangle_V + \langle \vartheta \rangle_S, \quad (2.11)$$

$$d_t \mathcal{E} = 2 \langle \mu S_{ij} S_{ij} \rangle_V - \langle \vartheta \rangle_S + \langle u_i f_i \rangle_V, \quad (2.12)$$

where  $\langle \cdot \rangle_S$  denotes the integral over the fluid-fluid. On average,  $\vartheta$  is the only term responsible for the exchange of surface and kinetic energies. We stress that these equations are valid independently of the physical properties of the fluids in the mixture, such as  $\rho$  and  $\mu$ , and only requires that the fluids are incompressible. Even in the case of different viscosities, the expression for  $\vartheta$  remains valid and is equally defined at both sides of the interface. In this case and in the sharp-interface limit, the balance of tangential stresses produces a discontinuity in the rate-of-strain tensor, but this only affects the off-diagonal components of the rate-of-strain tensor in a frame fixed to the interface, which do not enter  $\vartheta$  (Dopazo *et al.* 2000).

### 2.3. Inner and outer surface stretching

Despite the simplicity of the energetic exchange term, the coupling between the drop surface and the surrounding fluid is bidirectional and highly non-linear. To separate the inner dynamics of the drop from the action of the external velocity field, we split the surface-stretching term into inner and outer contributions by decomposing the rate-of-strain tensor as  $S_{ij} = S_{ij}^I + S_{ij}^O$ . Here  $S_{ij}^I$  is the rate-of-strain tensor induced on the surface of the drop by eddies close to and inside the drop, and  $S_{ij}^O$  by eddies away from

the drop surface. For this purpose, we define the outer vorticity field as

$$\boldsymbol{\omega}'^O = G(\mathbf{x}; \Delta) \boldsymbol{\omega}, \quad (2.13)$$

where

$$\begin{aligned} G(\mathbf{x}; \Delta) &= 1 \text{ if } |\mathbf{x} - \mathbf{x}_s| > \Delta \text{ and } \mathbf{x} \in \mathcal{O}, \\ G(\mathbf{x}; \Delta) &= 0 \text{ if otherwise,} \end{aligned} \quad (2.14)$$

is a kernel that defines the region outer to the the drop,  $\mathbf{x}_s$  defines the surface of the drop, and  $\mathcal{O}$  comprises all the points outside the drop. Let us note that  $\boldsymbol{\omega}'^O$  is not a vorticity field because it does not, in general, fulfill that  $\nabla \cdot \boldsymbol{\omega}^O = 0$ . We thus project it into the closest divergence-free field,  $\boldsymbol{\omega}^O = \boldsymbol{\omega}'^O - \nabla \psi$ , by solving

$$\nabla^2 \psi = \nabla \cdot \boldsymbol{\omega}'^O, \quad (2.15)$$

with periodic boundary conditions. The stretching induced on the drop by the eddies away from its surface can be calculated from the Biot–Savart law (Hamlington *et al.* 2008). By taking the curl of the vorticity and considering that  $\nabla \cdot \mathbf{u}^O = 0$ , we obtain the following equation

$$\nabla^2 \mathbf{u}^O = -\nabla \times \boldsymbol{\omega}^O, \quad (2.16)$$

whose solution (with periodic boundary conditions) provides the rate-of-strain tensor induced on the surface of the drop by eddies outside and inside the drop,  $S_{ij}^O = \frac{1}{2}(\partial_j u_i^O + \partial_i u_j^O)$  and  $S_{ij}^I = S_{ij} - S_{ij}^O$ .

The stretching of the drop surface due to vorticity at distances larger than  $\Delta$  from the drop surface is  $\vartheta^O = -n_i S_{ij}^O n_j$ , where the rate-of-strain tensor is evaluated at the surface of the drop, whereas  $\vartheta^I = -n_i S_{ij}^I n_j$  is the stretching induced by the flow field inside the drop and at a distance smaller than  $\Delta$  from the drop surface. A schematic representation of this decomposition is shown in figure 1(c).

### 3. Drop breakup in homogeneous isotropic turbulence

The analysis presented in the previous section is valid for any configuration of the fluid-fluid interface and for all flow regimes. The central role of the rate-of-strain tensor in our analysis is consistent with experiments and theoretical analyses of laminar flows in the Stokes limit. As noted by Rallison (1984): “Drop deformation and burst is promoted primarily by the straining motion in the external shear. It is inhibited by the vorticity in the outer flow.”. Hereinafter we apply our analysis to the dynamics of a single drop embedded in a homogeneous and isotropic turbulent flow.

#### 3.1. Numerical methods

We consider two fluids with equal density and kinematic viscosity, and integrate (2.1) in a triply periodic domain of volume  $L^3 = (2\pi)^3$  by projecting the equations on a basis of  $N/2$  Fourier modes in each direction, where  $N = 256$ . Non-linear terms are computed through a dealiased pseudo-spectral procedure, and a third-order semi-implicit Runge-Kutta scheme is used for the time integration, with a decomposition of the linear terms proposed by Badalassi *et al.* (2003). To sustain turbulence in a statistically steady state, we implement a linear body-force,  $\hat{f}_i = C_f \hat{u}_i$ , that is only applied to wavenumbers  $k < 2$ , where  $\hat{\cdot}$  denotes the Fourier transform and  $k$  is the wavenumber magnitude. The forcing coefficient  $C_f$  is set so that, at each time, the total kinetic energy per unit time injected in the system is constant and equal to  $\varepsilon$ , while the kinematic viscosity  $\nu = \mu/\rho$  is tuned to keep a prescribed numerical resolution,  $k_{max}\eta = 4$ , where  $\eta = (\nu/\varepsilon^4)^{3/4}$  is

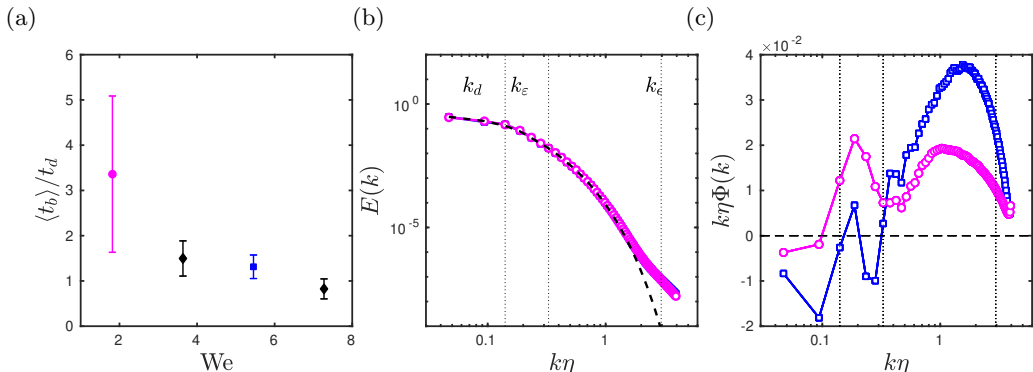


FIGURE 2. (a) Average time to breakup as a function of the  $We$ . The upper and lower bars mark the standard deviation. (b) Kinetic energy spectra at  $Re_\lambda = 58$  for : ---, turbulent flow without droplet; —○—,  $We = 1.8$ ; —□—,  $We = 5.4$ . Vertical dotted lines mark the scale of the drop,  $k_d = 2\pi/d$ , the scale where the spectral density of the kinetic energy dissipation is the highest,  $k_\varepsilon$ , and the scale of the interface,  $k_\epsilon = 2\pi/\epsilon$ . (c) Pre-multiplied production spectra,  $k\eta\Phi(k)$ . Lines as in (a). The total contribution of each wavenumber to the variation of the surface free energy is represented as the area below the curve.  $\Phi$  is normalized with its average in each case.

the Kolmogorov length scale and  $k_{max} = N/3$  is the maximum wavenumber magnitude after dealiasing.

The Reynolds number of the flow is  $Re_\lambda = \lambda u' / \nu = 58$ , where  $\lambda = \sqrt{15(\nu/\varepsilon)}u'$  is the Taylor microscale,  $u' = \sqrt{3\mathcal{E}/2}$  is the root-mean-square of the velocity fluctuations, and  $\mathcal{E} = 1/2\langle u_i u_i \rangle$  is the ensemble-averaged kinetic energy. The thickness of the fluid-fluid interface is set by the Cahn number  $Cn = (\alpha/\beta L^2)^{1/2} = 0.012$ , which for  $N = 256$  is appropriate to resolve the interface with a spectral Fourier basis (Chen & Shen 1998), and the mobility enters the Peclet number of  $Pe = u' L^2 / \kappa \sqrt{\alpha\beta} = 3Cn^{-2}$  (Magaletti *et al.* 2013). The time-step is set to  $\Delta t = 0.04Cn$ . Simulations have been performed on GPUs using a modified version of the spectral code described in Cardesa *et al.* (2017). The code has been validated against Shao *et al.* (2018), and the consistency of the numerical parameters, such as the time-step and the spatial resolution, have been checked.

### 3.2. Initial conditions and drop size

We introduce a drop of diameter  $d = \frac{1}{3}L$  in a fully developed turbulent flow, and integrate the governing equations (2.1) until the drop breaks (see figure 1(d)). Since  $d = 45\eta$ , breakup is dominated by inertial forces and characterized by the Weber number,  $We = \rho \varepsilon^{2/3} d^{5/3} / \sigma$ , and by a characteristic inertial time-scale  $t_d = (d^2 \varepsilon)^{1/3}$ . To statistically characterise drop deformation and breakup, we perform many independent single-drop simulations initialized with statistically independent turbulent flow fields. Mass leakage (Yue *et al.* 2007) leads to a progressive reduction of the drop diameter, and to a time-dependent average Weber number,  $We(t)$ , which decreases slightly through the simulations. We consider the effective Weber number of our simulations as the average Weber number at the average time of breakup,  $\langle t_b \rangle$ , i.e  $We = \langle We(\langle t_b \rangle) \rangle$ . The difference of the Weber number at the time of breakup with respect to the measured Weber number due to shrinkage is at most  $\sim 3\%$  in the worst cases.

We performed simulations at four different effective  $We$  in the range of  $1.8 - 7.4$ . The total number of simulations is about 100 for each  $We$ , which yield a total simulation time of between  $300t_d$  and  $1500t_d$ . From each simulation, we stored full flow fields with adequate temporal resolution to have fully converged statistics. In figure 2(a), we show

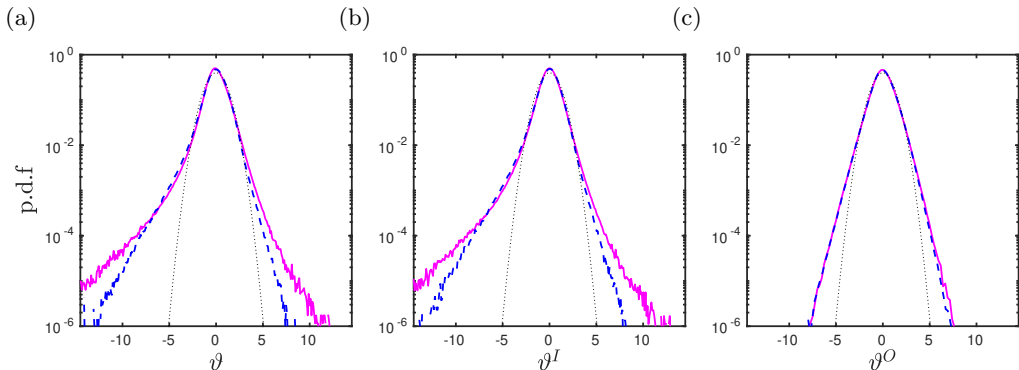


FIGURE 3. Probability density function of  $\vartheta$  calculated with the full (a), the inner (b) and the outer (c) rate-of-strain tensor for  $\Delta = 6\eta$ . Lines correspond to: —,  $We = 1.8$ ; ---,  $5.4$ . The black dotted line corresponds to a Gaussian. Probability density functions centered at the mean, and  $\vartheta$ ,  $\vartheta^I$  and  $\vartheta^O$  normalised with their respective standard deviations.

the mean and the standard deviation of the time to breakup,  $t_b$ , as a function of the  $We$ . As expected, low values of  $We$ , the longer the time it takes for breakup to occur.

In what follows we show that although  $d$  is comparable to the integral scale of the flow, the drop does neither modify the structure of the surrounding turbulence nor resonate with the numerical box. The drop interacts mostly with scales smaller than  $d$ , indicating that the linear forcing used to sustain turbulence does not affect breakup. In figure (2a), we show the average kinetic energy spectrum,  $E(k) = 2\pi k^2 \langle \hat{u} \hat{u}^* \rangle_k$ , with and without an immersed drop. Here  $\langle \cdot \rangle_k$  denotes averaging over modes with wavenumber magnitude  $k$ , and  $\cdot^*$  represents the complex conjugate. The energy spectra is similar for the flow with and without droplet above  $k\eta \sim 1$ , indicating healthy turbulent dynamics in those scales. The good collapse of the energy spectra in the small wavenumbers also suggests the absence of any resonances between the drop and the box, which could lead to spurious large-scale dynamics. To examine how the large-scale forcing affects the dynamics of breakup, we study the pre-multiplied production spectra

$$\Phi(k) = -4\pi k^2 \Re \langle \widehat{(u_j \partial_j c)} \hat{\phi}^* \rangle_k, \quad (3.1)$$

which describes the contribution of each scale to the changes of the surface energy due to the deformation of the interface by the velocity field. In figure 2(b), we show that variations of the surface energy are due mostly to turbulent fluctuations in the small scales of the flow, whereas the contribution of the large scales is small compared to the rest. In fact, the contribution of the scales affected by the forcing (with  $k < 2$ ) to the production of surface energy is slightly negative on average, confirming that the forcing does not contribute to breakup.

#### 4. Statistics of the energetic exchange

We now use the decomposition presented in §2.3 to study the local stretching of the drop surface due to eddies close to, or away from, the drop surface. Without aiming at a rigorous physical definition, we refer to these eddies as inner and outer eddies respectively, and use values of  $\Delta$  in the range from  $6\eta$  to  $9\eta$ , for which their contributions to the local stretching are very distinct. In figure 3(a-c), we show the probability density function (p.d.f) of  $\vartheta$ ,  $\vartheta^O$ , and  $\vartheta^I$  for  $We = 1.8$  and  $5.4$  and  $\Delta = 6\eta$ . We find that  $\vartheta$  and  $\vartheta^I$  are very similar and display fairly fat-tailed distributions which depend on the  $We$ .

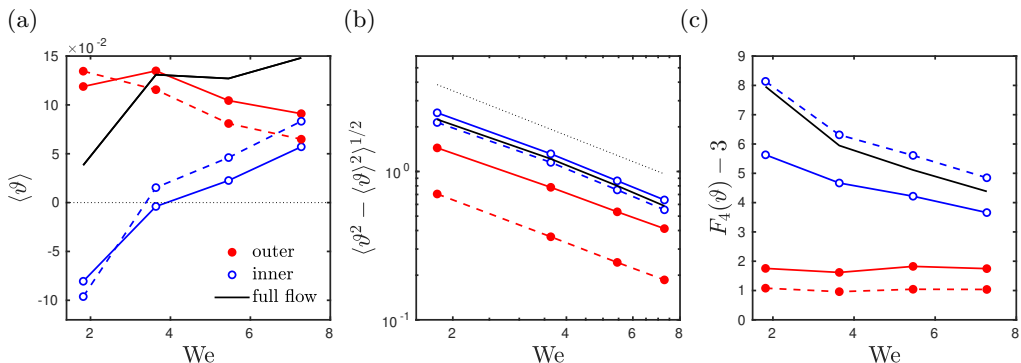


FIGURE 4. (a) Mean, (b) standard deviation, and (c) excess flatness of  $\vartheta$  as a function of  $We$ . Mean and standard deviation normalized with  $\rho u_d^3$ . The flatness is defined as  $F_4(\vartheta) = \langle (\vartheta - \langle \vartheta \rangle)^4 \rangle / \langle \vartheta^2 - \langle \vartheta \rangle^2 \rangle^2$  and the excess flatness is the flatness with respect to a Gaussian distribution, for which  $F_4 = 3$ . Solid symbols corresponds to the statistics of  $\vartheta^O$ , and empty symbols to  $\vartheta^I$ . Color lines correspond to  $\Delta =$ : —,  $6\eta$ ; ---,  $9\eta$ ; and solid black line to the full rate-of-strain tensor. In (b) the dotted line is proportional to  $We^{-1}$ .

Their prominent negative tails indicate the presence of intense relaxation events. By contrast,  $\vartheta^O$  is symmetric, closer to a Gaussian and its shape is independent of the  $We$ . In figure 4(a), we show the mean of  $\vartheta$ ,  $\vartheta^O$ , and  $\vartheta^I$  for different values of  $We$  and  $\Delta$ . In all cases, the average contribution of the outer eddies to the stretching of the interface is larger than, or at least comparable to, the inner contribution. The average increment of surface energy changes with  $We$ , but this variation is due mostly to changes in the dynamics close to the drop surface, which transitions from  $\langle \vartheta^I \rangle < 0$  to  $\langle \vartheta^I \rangle > 0$  as  $We$  increases, suggesting that the flow inside or near the surface of the drop becomes turbulent at sufficiently large  $We$ . On the other hand, the average contribution of the outer eddies to the stretching of the surface remains fairly constant with  $We$ . Since the increment of the surface energy directly relates to drop breakup, we suggest that, even at the largest  $We$ , an important part of the breakup is caused by the action of surrounding turbulence more than  $\sim 9\eta \approx 0.2d$  away from the drop surface.

In figure 4(b), we show that the standard deviation of  $\vartheta$  is approximately proportional to  $We^{-1}$  in all cases, and substantially higher for the inner than for the outer contributions. This implies that, as the  $We$  decreases, the fluctuations of the local surface stretching become much higher than the mean, suggesting that most of the stretching is not efficient, and cancels out when averaging. The flatness factor, shown in figure 4(c), also reflects the differences between the outer and inner contributions. For the former it is independent of the  $We$ , while for the latter it increases with decreasing  $We$ .

We explain the statistical differences between the inner and outer contributions by studying the structure of the rate-of-strain tensor induced by inner and outer eddies, and of the vorticity vector, at the surface of the drop. In figure 5(a)–(c), we show the p.d.f of the cosine of the angle of alignment between each of the principal axes of the rate of strain tensor,  $\mathbf{v}_1$ ,  $\mathbf{v}_2$  and  $\mathbf{v}_3$ , where  $\lambda_1 > \lambda_2 > \lambda_3$  are their corresponding eigenvalues, and the normal to the surface,  $\mathbf{n}$ .

For the inner contributions, the most stretching ( $\mathbf{v}_1$ ) and the most compressing ( $\mathbf{v}_3$ ) eigenvectors tend to be oriented at  $\sim 45^\circ$  with respect to the surface normal. The intermediate eigenvalue is parallel to the surface. This alignment is stronger for lower  $We$ , indicating that it is caused by surface tension forces. This is consistent with the strong alignment of the vorticity vector parallel to the surface (see figure 5(d)), which is most probably caused by the oscillations of the surface during the relaxation of the drop.



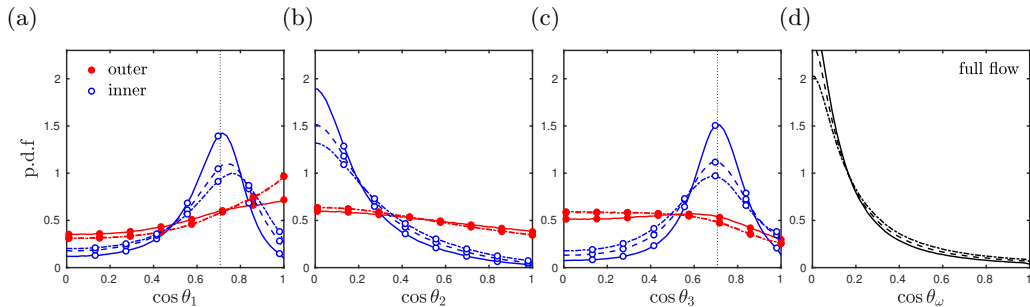


FIGURE 5. (a-c) Probability density function of  $\cos \theta_i = \mathbf{n} \cdot \mathbf{v}_i$ , where  $\mathbf{v}_i$  are the principal directions of the rate of strain tensor and  $\lambda_1 > \lambda_2 > \lambda_3$  are their eigenvalues. Solid markers correspond to angles calculated with the inner flow field, and empty markers to the outer field for  $\Delta = 9\eta$ . (d) Similar but for the vorticity vector of the full flow field,  $\cos \theta_\omega = \mathbf{n} \cdot \boldsymbol{\omega}/|\boldsymbol{\omega}|$ . Lines correspond to  $We =$ : —, 1.8; ---, 3.6; - · -, 5.4. The vertical dotted line in (a) and (c) marks  $\cos \pi/4$ .

We note that the surface cannot generate vorticity normal to it due to  $\mathbf{n} \cdot \nabla \times (\phi \nabla c) = 0$ . The outer contributions to the stretching of the surface show a substantially different picture. There is a consistent tendency of the most compressing eigenvalue to align normal to the interface, although in this case the alignment is less marked. The good collapse at different  $We$  suggest that this tendency is roughly independent of the surface dynamics.

## 5. Discussion

The outer drop dynamics is relevant for deformation and breakup at all  $We$  and depends mostly on the structure of the surrounding turbulence. On the other hand, the inner contributions are only relevant at high  $We$ . The latter are dominated by surface dynamics, and display  $We$ -dependent statistics. The very different qualitative nature of inner and outer dynamics, and the disparate scaling of their contributions to surface energy increments and high order statistics, suggest that they are largely decoupled, and that they may be considered separately. Hence a ‘random’ approach to model breakup appears to be justified since the outer and inner dynamics are not expected to be synchronized, precluding any synergies or coupling that may lead to enhanced breakup. Our results rule out, at least for the case of equal density and viscosity, the possibility of a breakup caused by drop-induced oscillations as observed by Risso & Fabre (1998) in their experiments of bubbly flows under microgravity conditions.

We have reported a statistically significant alignment of the surface normal with the most compressing direction of the non-local rate-of-strain tensor. This phenomenon, which is also observed in the evolution of material surfaces in turbulence and naturally leads to the alignment of both vectors (Girimaji & Pope 1990), indicates the persistent stretching of the drop surface by outer eddies. This appears as a plausible mechanism for drop breakup, and constitutes a reinterpretation of the phenomenological ‘collision’ of eddies. The statistics show that much of this stretching is not efficient. A possible picture is that weak background turbulence produces much of this inefficient stretching, while the most intense structures produce the stretching leading to breakup.

To conclude, let us remark that we have also identified a secondary breakup mechanism at large  $We$ , when the flow inside and at the surface of the drop seems to become turbulent and contributes substantially to breakup. This mechanism is probably inhibited in drops with viscosity larger than that of the surrounding fluid, which may explain their resistance to breakup (Calabrese *et al.* 1986; Roccon *et al.* 2017).

## Acknowledgements

A.V-M acknowledges the support of the European Research Council COTURB project ERC-2014.AdG-669505.

## REFERENCES

- AIYER, A.K., YANG, D., CHAMECKI, M. & MENEVEAU, C. 2019 A population balance model for large eddy simulation of polydisperse droplet evolution. *J. Fluid Mech.* **878**, 700–739.
- BADALASSI, V. E., CENICEROS, H. D. & BANERJEE, S. 2003 Computation of multiphase systems with phase field models. *J. Comput. Phys.* **190** (2), 371–397.
- CALABRESE, R.V., CHANG, T.P.K. & DANG, P.T. 1986 Drop breakup in turbulent stirred-tank contactors. Part I: Effect of dispersed-phase viscosity. *AIChE J.* **32** (4), 657–666.
- CARDESA, J.I., VELA-MARTÍN, A. & JIMÉNEZ, J. 2017 The turbulent cascade in five dimensions. *Science* **357** (6353), 782–784.
- CHEN, L.Q. & SHEN, J. 1998 Applications of semi-implicit fourier-spectral method to phase field equations. *Comput. Phys. Commun.* **108** (2), 147–158.
- DOPAZO, C., LOZANO, A. & BARRERAS, F. 2000 Vorticity constraints on a fluid/fluid interface. *Phys. Fluids* **12** (8), 1928–1931.
- EASTWOOD, C. D., ARMI, L. & LASHERAS, J. C. 2004 The breakup of immiscible fluids in turbulent flows. *J. Fluid Mech.* **502**, 309333.
- GIRIMAJI, S.S. & POPE, S.B. 1990 Material-element deformation in isotropic turbulence. *J. Fluid Mech.* **220**, 427–458.
- HAKANSSON, A. 2019 Emulsion formation by homogenization: Current understanding and future perspectives. *Annu. Rev. Food Sci. Technol.* **10** (1), 239–258.
- HAMLINGTON, P.E., SCHUMACHER, J. & DAHM, W.J.A. 2008 Local and nonlocal strain rate fields and vorticity alignment in turbulent flows. *Phys. Rev. E* **77** (2), 026303.
- HINZE, J.O. 1955 Fundamentals of the hydrodynamic mechanism of splitting in dispersion processes. *AIChE Journal* **1** (3), 289–295.
- JACQMIN, D. 1999 Calculation of two-phase Navier–Stokes flows using phase-field modeling. *J. Comput. Phys.* **155** (1), 96–127.
- KOLMOGOROV, A.N. 1949 On the disintegration of drops in turbulent flow. In *Doklady Akad. Nauk. USSR*, , vol. 66, p. 825.
- LASHERAS, J.C., EASTWOOD, C., MARTINEZ-BAZÁN, C. & MONTANES, J.L. 2002 A review of statistical models for the break-up of an immiscible fluid immersed into a fully developed turbulent flow. *Int. J. Multiph. Flow* **28** (2), 247–278.
- LIAO, Y. & LUCAS, D. 2009 A literature review of theoretical models for drop and bubble breakup in turbulent dispersions. *Chem. Eng. Sci.* **64** (15), 3389–3406.
- MAASS S. & KRAUME, M. 2012 Determination of breakage rates using single drop experiments. *Chem. Eng. Sci.* **70**, 146 – 164.
- MAGALETTI, F., PICANO, F., CHINAPPI, M., MARINO, L. & CASCIOLA, C. M. 2013 The sharp-interface limit of the Cahn–Hilliard/Navier–Stokes model for binary fluids. *J. Fluid Mech.* **714**, 95–126.
- RALLISON, J.M. 1984 The deformation of small viscous drops and bubbles in shear flows. *Annu. Rev. Fluid Mech.* **16** (1), 45–66.
- RISSO, F. & FABRE, J. 1998 Oscillations and breakup of a bubble immersed in a turbulent field. *J. Fluid Mech.* **372**, 323–355.
- ROCCON, A., DE PAOLI, M., ZONTA, F. & SOLDATI, A. 2017 Viscosity-modulated breakup and coalescence of large drops in bounded turbulence. *Phys. Rev. Fluids* **2** (8), 083603.
- SHAO, CHANGXIAO, LUO, KUN, YANG, YUE & FAN, JIANREN 2018 Direct numerical simulation of droplet breakup in homogeneous isotropic turbulence: The effect of the weber number. *Int. J. Multiph. Flow* **107**, 263–274.
- YUE, P., ZHOU, C. & FENG, J. J. 2007 Spontaneous shrinkage of drops and mass conservation in phase-field simulations. *J. Comput. Phys.* **223**, 1–9.